ADVANCED MATERIALS
www.advmat.de

Intracellular Condensates of Oligopeptide for Targeting Lysosome and Addressing Multiple Drug Resistance of Cancer

*Jing Wang, Liangbo Hu, Hongyue Zhang, Yu Fang, Tingliang Wang, and Huaimin Wang**

Biomolecular condensates have been demonstrated as a ubiquitous phenomenon in biological systems and play a crucial role in controlling cellular functions. However, the spatiotemporal construction of artificial biomolecular condensates with functions remains challenging and has been less explored. Herein, a general approach is reported to construct biomolecular condensates (e.g., hydrogel) in the lysosome of living cells for cancer therapy and address multiple drug resistance induced by lysosome sequestration. Aromatic-motif-appended pH-responsive hexapeptide (LTP) derived from natural insulin can be uptaken by cancer cells mainly through caveolae-dependent endocytosis, ensuring the proton-triggered phase transformation (solution to hydrogel) of LTP inside the lysosome specifically. Lysosomal hydrogelation further leads to enlargement of the lysosome in cancer cells and increases the permeability of the lysosome, resulting in cancer cell death. Importantly, lysosomal assemblies can significantly improve the efficiency of current chemotherapy drugs toward multidrug resistance (MDR) cells in vitro and in xenograft tumor models. As an example of functional artificial condensates in lysosomes, this work provides a new strategy for controlling functional condensates formation precisely in the organelles of living cells and addressing MDR in cancer therapy.

1. Introduction

Molecular self-assembly, a prevalent phenomenon used extensively in nature, serves as a bottom-up approach in chemistry and materials science to generate functional structures.[1,2] Although research in this field has achieved great successes in constructing functional biomaterials in vitro in a variety of applications,[3–11] instructed self-assembly for cancer therapy and imaging, which involves the endogenous stimuli and molecular self-assembly to form functional higher-order structures in living cells, has emerged as a promising strategy in the past decade.[12–20] Living cells used this strategy to make functional macromolecules involving highly efficient catalytic reactions (e.g., enzyme, redox, pH) and then self-assemble to form higher-order structures.[21] Recent discoveries also highlight the essential role of intracellular condensed liquid-like droplets (e.g., hydrogel in most cases) of biomolecules, including protein and RNA, in dictating the biological functions and devastating diseases.[22–25] Thus, a synthetic platform of functional higher-order assemblies (e.g., hydrogel) in living cells could offer an opportunity to understand the intracellular condensates and perform certain functions.[26–28]

Since Coffey and De Duve's discovery of the lysosome,[29,30] the lysosome has been recognized as an essential cellular organelle (or recycling center) to degrade and recycle extracellular and intracellular materials.[31] The dysfunction of the lysosome has been implicated in many diseases, including cancer progression. Understanding the function and dysfunction of the lysosome in recent years suggests the targeting lysosome selectively emerges as a novel opportunity for treating diseases. For example, heat-shock protein 70 (HSP70) and V-H$^+$-ATPase are attractive targets in the drug screening for cancer treatment by increasing lysosomal pH and inducing lysosomal-membrane permeabilization (LMP).[32] Moreover, the acidic property of the lysosomal compartment of tumor cells is usually used to modulate drug release from acid-sensitive prodrug or pH controllable drug carriers.[33,34] Although the above strategies have achieved remarkable success for therapeutically targeting the lysosome, less attention has been focused on forming functional assemblies inside lysosome through molecule self-assembly.[35,36] Moreover, lysosomal drug sequestration contributes to cancer multidrug resistance by entrapping chemotherapeutic agents in lysosome to reduce drug availability to sites of action.[37,38] We hypothesized that in situ construction of biomolecular condensates in the lysosome could change the lysosomal property and

J. Wang, L. Hu, H. Zhang, Y. Fang, H. Wang
Key Laboratory of Precise Synthesis of Functional Molecules of Zhejiang Province
School of Science
Westlake University
Institute of Natural Sciences
Westlake Institute for Advanced Study
18 Shilongshan Road, Hangzhou, Zhejiang Province 310024, China
E-mail: wanghuaimin@westlake.edu.cn
J. Wang, T. Wang, H. Wang
Westlake Laboratory of Life Sciences and Biomedicine
School of Life Sciences
Westlake University
Hangzhou, Zhejiang 310024, China
The ORCID identification number(s) for the author(s) of this article can be found under https://doi.org/10.1002/adma.202104704.

DOI: 10.1002/adma.202104704

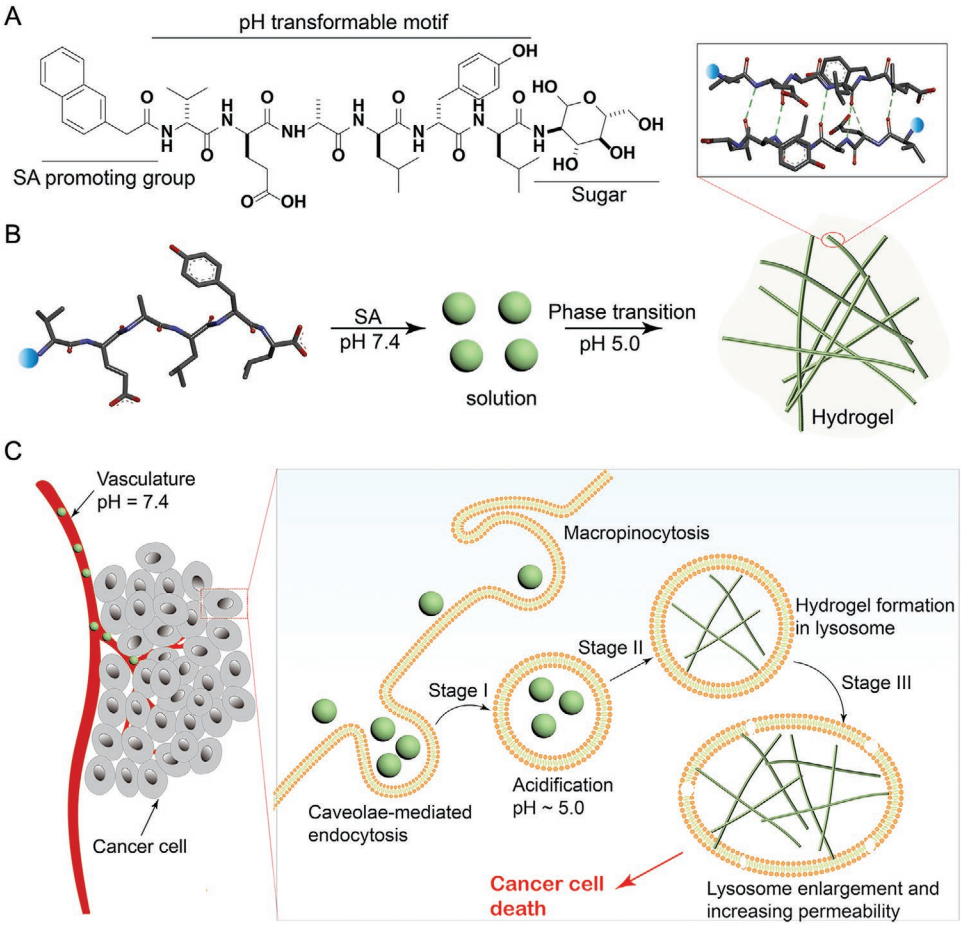

Figure 1. Schematic illustration of pH-responsive transformable peptides and the self-assembly process in vitro and in vivo. A) Typical molecular structure of LTP which composed of a SA promoting group, a pH transformable motif and C-terminal modification with or without sugar. B) LTP could form nanoparticles at pH 7.4 aqueous solution and transform into nanofibers in acidic condition (pH 5.0) through noncovalent interaction, which further entangled with each other to form self-supporting hydrogel. C) Phase-transformation process in living cells. After being uptaken by cancer cells through endocytosis (stage I), oligomers of LTP accumulate in the lysosomes and transform into nanofibrous hydrogel through proton-induced phase transformation (stage II). The nanofibrous hydrogel further induces the enlargement of the lysosome (stage III) and causes LMP to result in cancer cell death.

redirect the lysosomal sequestrated drugs to the active targets for addressing MDR.

Here, we report a general approach that could induce functional assemblies (e.g., hydrogel) formation in the lysosome of living cells (**Figure 1**). Taken advantage of lysosomal acidification and a pH-responsive natural protein, we rationally designed aromatic capped peptides that reversibly form higher-order assemblies from oligomers with the changing of conformation and morphologies in the lysosome. The oligomer of molecules could readily uptake by cells mainly through caveolae-mediated endocytosis. The proton in lysosome then induces the self-assembly of molecules to form a nanofibrous hydrogel, as evidenced by in vitro and in vivo experiments. The lysosomal hydrogel undergoes swelling in the lysosome, leading to massive lysosome swelling, resulting in cancer cell death through necroptosis and apoptosis. Significantly, the lysosome swelling also changes the lysosomal membrane's permeability and releases the trapped chemotherapy drugs to the cytosol, resulting in over 600 folds of bioactivity. Using two drug-resistant tumor-bearing mouse models, we demonstrate that our strategy could inhibit drug-resistant cancer growth during the therapeutic period. This work, mimicking the functional high-order assemblies (e.g., biomolecular condensates) in cells, opens up a new opportunity for addressing multidrug drug resistance of cancer.

2. Results and Discussion

2.1. Design, Synthesis, and Characterization of Lysosomal Acid-Induced Assemblies

Based on the concept illustrated in Figure 1, the designed lysosome targeting molecule (LTP) consists of the following essential parts: i) Val–Glu–Ala–Leu–Tyr–Leu (VEALYL)[39] is the segment derived from human insulin protein, which plays a crucial role in determining the aggregation of insulin. A detailed mechanistic study suggested that this segment could form amyloid fibrils consisting of a pair of β-sheet through intermolecular hydrogen bonding.[39] Eisenberg and others

demonstrated that the aggregation of this segment depends on the changes of pH.[39,40] LTP forms amyloid fibers (or microcrystals) under acidic conditions while remains in the soluble oligomer state at neutral pH. Taking advantage of the property of this segment, we thus select VEALYL as a pH-responsive segment in our design. ii) *N*-terminal modification of the 2-naphthylacetyl group provides the aromatic–aromatic interaction to increase the self-assembly ability of peptides.[41] iii) C-terminal glycosylation of peptide to improve the proteolytic stability of peptides. We used the standard Fmoc-based solid-phase peptide synthesis (SPPS) to synthesize L (L-LTP) and D (D-LTP) enantiomer of LTP. After obtained the LTP, we used liquid phase coupling to synthesize glycopeptide (**Figure 2**A), resulting in L-LTPS and D-LTPS. All the molecules were purified by high-performance liquid chromatography (HPLC), and analyzed by ^{1}H NMR spectra and LC–MS to confirm the

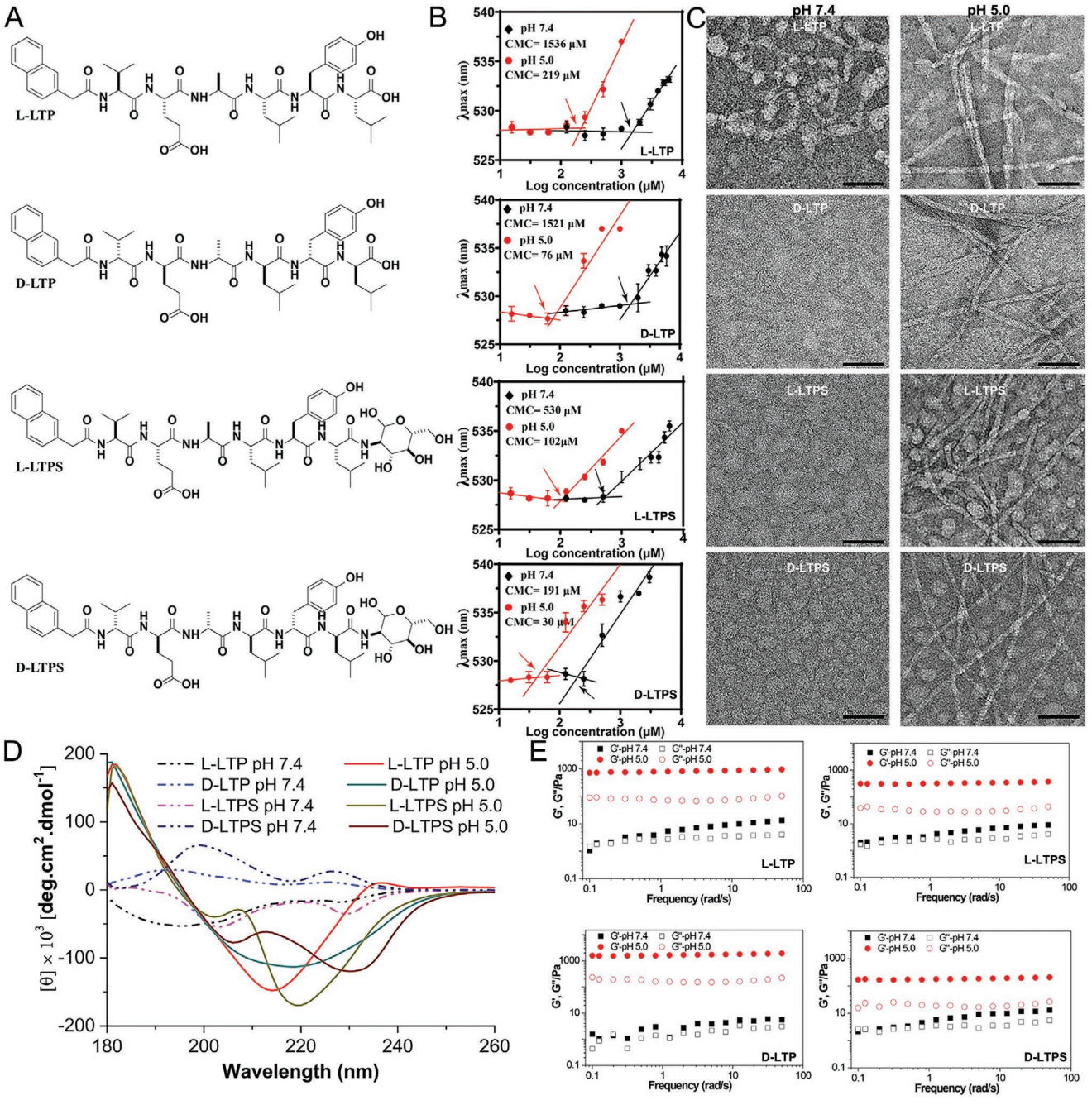

Figure 2. Physiochemical characterization of self-assembling behavior of designed molecules in this work. A) Molecular structure of peptides L-LTP, D-LTP, L-LTPS, and D-LTPS. B) CMC values of L-LTP, D-LTP, L-LTPS, and D-LTPS at pH 7.4 and pH 5.0 that measured by the Rhodamine 6G method. C) TEM images of L-LTP, D-LTP, L-LTPS, and D-LTPS at the concentration of 500×10^{-6} M at pH 7.4 and pH 5.0. Scale bar: 100 nm. D) CD spectra of L-LTP, D-LTP, L-LTPS, and D-LTPS (500×10^{-6} M) at pH 7.4 and pH 5.0. E) Rheological measurement of L-LTP, D-LTP, L-LTPS, and D-LTPS at the concentration of 5×10^{-3} M at pH 7.4 and pH 5.0.

structures and purities (Figures S1–S3 and Table S1, Supporting Information).

To examine the pH-responsive property of the molecules, we first measured their critical micellization concentration (CMC) at different pHs since CMC reflects the self-assembling abilities of a given molecule. The results (Figure 2B) show that the CMC value of L-LTP reduced from 1536 to 219×10^{-6} M with a pH change from 7.4 to 5.0, which is over seven folds reduction. The CMC value of D-LTP follows a similar trend, which is 1521×10^{-6} M at pH 7.4 and decreases to 76×10^{-6} M at pH 5.0. Notably, the CMC value of L-LTPS (or D-LTPS) is 530×10^{-6} M (or 191×10^{-6} M) at pH 7.4, indicating C-terminal modification of LTP increases the self-assembly ability of resulted molecules. At pH 5.0, the CMC value of L-LTPS and D-LTPS is 102×10^{-6} M (five folds reduction) and 30×10^{-6} M (six folds reduction), suggesting the glycosylation of LTP maintains the pH-responsive property of original peptides. Stability analysis experiments indicate that D-LTP and D-LTPS are stable in proteinase K solution (1.0 mg mL^{-1}) and 10% fetal bovine serum (FBS) solution (Figure S9, Supporting Information). We also found that L-LTP and L-LTPS are easy to be degraded compared with D-LTP and D-LTPS. L-LTP almost degraded completely in proteinase K (1.0 mg mL^{-1}) and 10% FBS solution after 2 h incubation, while the glycosylated peptide L-LTPS is much more stable than L-LTP since 48% of L-LTPS still maintained in 10% FBS after 24 h incubation. Transmission electron microscopy (TEM) images reveal the pH-dependent morphology transformation of these molecules at different pHs (Figure 2C). These molecules self-assembled into nanoparticles at pH 7.4. While an acidic environment can deionize the carboxyl group and enhance the self-assembly of the molecules to transform into nanofibers. Statistical image analysis shows that the mean diameter of nanofibers is 10.28 ± 1.42 nm for L-LTP, 11.38 ± 2.03 nm for D-LTP, 9.51 ± 1.00 nm for L-LTPS, and 7.51 ± 0.88 nm for D-LTPS, respectively. TEM images (Figure S4, Supporting Information) also show that the transformation of nanoparticles to nanofibers starts at pH 6.0. The nanoparticles are stable within the pH range from 7.4 to 8.2, and the nanofibers are very stable at pH 4.0–6.0. The results of dynamic light scattering (DLS, Figure S5, Supporting Information) also consist with the morphology change that observed by TEM, further demonstrating that the changing of environmental pH induces the morphology transformation of peptide. We further used atomic force microscopy (AFM), Cryo-EM, and DLS to characterize the self-assembly property of our peptides (Figures S6–S8, Supporting Information). The results of AFM show the morphology transformation of the peptides in pH 7.4 and pH 5.0 solution, agreeing with the observation by TEM. To better understand the self-assembly property of the peptide without drying effects, we used Cryo-EM to examine the morphology of peptides at different pHs. The results show that the peptides form nanospheres in pH 7.4 and nanofibers in pH 5.0, consisting with the observation by AFM. DLS results indicate that peptides in pH 5.0 have longer timescales of inflection points in Autocorrelation function profiles than in pH 7.4, which confirms the transformation from oligomer to nanofibers of peptides. Circular dichroism (CD) results reveal the conformation changes of peptide at different pHs. Compared with the peptide at pH 7.4, there is one negative peak at 214 nm (L-LTP) and 218 nm (D-LTP), and one positive peak at 181 nm in pH 5.0. For glycosylated peptide of LTPS, the CD spectra show one positive peak at 181 nm and two negative peaks at 206 and 219 nm (Table S2, Supporting Information). These results suggest that the designed peptides undergo pH-dependent conformational changes. To investigate whether the molecules could undergo a phase transformation from solution to hydrogel in living cells under the acidic condition, we first performed the hydrogelation test in vitro at different pHs by GdL strategy.[42] GdL strategy is widely used to prepare the hydrogel by pH adjustment, which hydrolyzes glucono-δ-lactone to generate gluconic acid and results in pH gradient of the system. The results show that all the molecules could form transparent hydrogel at pH 5.0, while maintaining a clear solution at pH 7.4, suggesting the pH-dependent phase transition of the molecules, which is consistent with the observation of TEM images. According to the results of critical gelation concentration (CGC) experiments (Figure S10, Supporting Information), the CGC of D-LTP and D-LTPS is 1.0×10^{-3} M. Rheological experiments (Figure 2E) reveal that the storage modulus (G') is almost the same as the loss modulus (G'') of molecules at pH 7.4, which is lower than 30 Pa. In contrast, all the molecules form hydrogel at pH 5.0 at the same concentration, as evidenced by the dominating value of G' in the rheological measurement. These results suggest that the designed molecules could form stable hydrogel under an acidic environment similar to the pH value of lysosome, suggesting the promising formation of hydrogel in the lysosome of living cells.

2.2. Intracellular Formation and Distribution of Molecular Assemblies

We next evaluate the bioactivity of the intracellular molecular assemblies on human cervical cancer (HeLa) cells. As shown in **Figure 3**A, L-LTP has little cytotoxicity against HeLa cells, and D-LTP kills about 50% HeLa cells at high concentration (500×10^{-6} M), while L-LTPS and D-LTPS exhibit higher cytotoxicity toward HeLa cells in a concentration-dependent manner. The IC_{50} of D-LTPS is 343×10^{-6} M (24 h) and 196×10^{-6} M (48 h) against HeLa cells. While for L-LTPS, cell viability is higher than that of D-LTPS after 48 h incubation, indicating that D-LTPS still show decent inhibitory effect even after 48 h incubation (Figure S11, Supporting Information). These results together indicate that the stability and self-assembling ability of molecules together determine the cytotoxicity of final assemblies. Apoptosis/necrosis assay by flow cytometry suggests that the cell death induced by D-LTPS involved both apoptosis and necrosis (Figure 3B). Moreover, we also utilized necroptosis inhibitor Necrostatin-1 (Nec-1)[43,44] and caspase inhibitor Z-VAD-FMK[45] to investigate the modality of cell death induced by molecular assemblies (Figure S12, Supporting Information). The cytotoxicity results indicate that Z-VAD-FMK could rescue the cell viability of HeLa cells from 78% to 116% upon the treatment with D-LTP (200×10^{-6} M) for 24 h, while the cytotoxicity of D-LTPS is barely reduced (200×10^{-6} M) with addition of Z-VAD-FMK. However, Nec-1 decreases the cytotoxicity of both D-LTP and D-LTPS in a concentration-dependent manner,

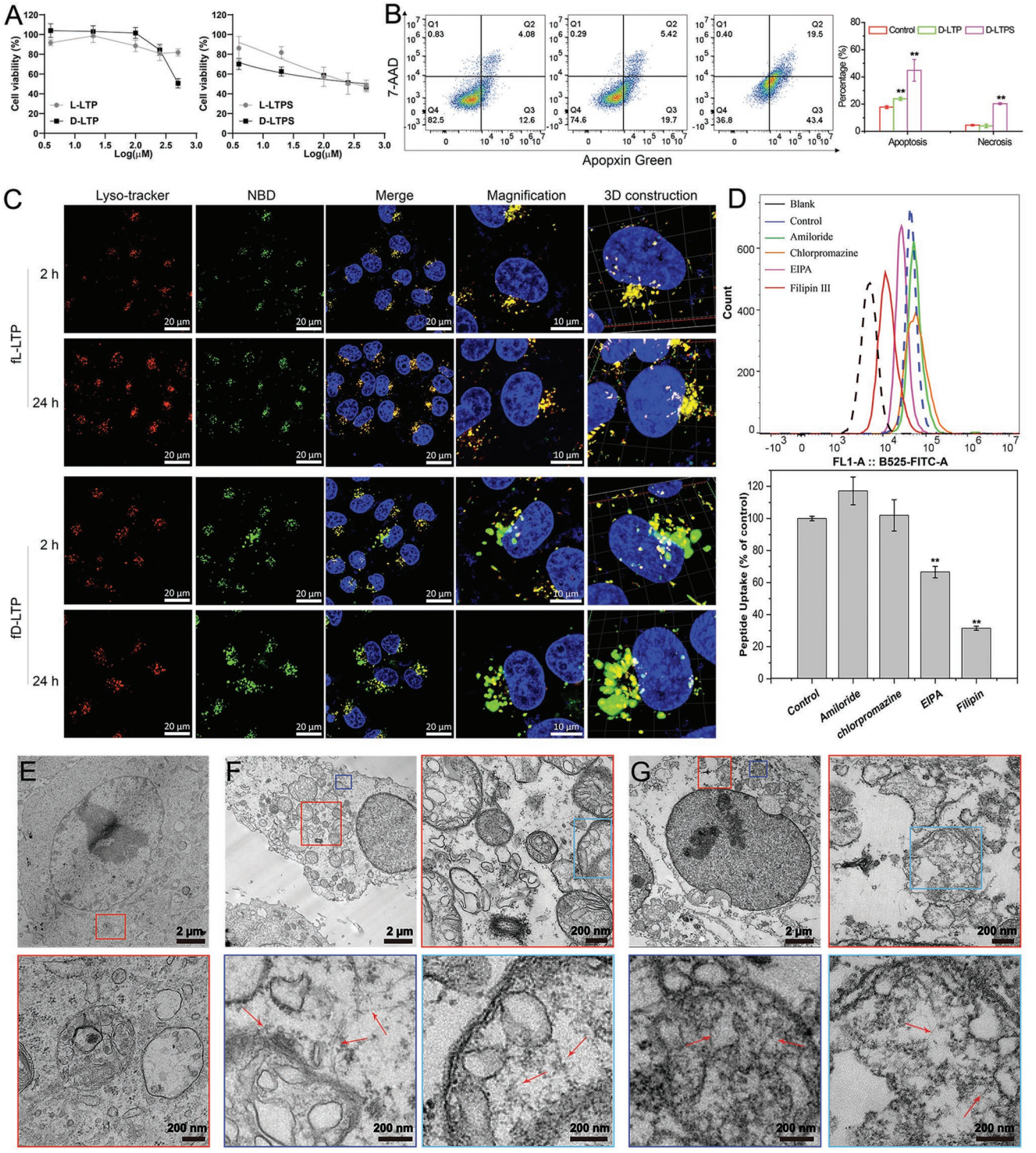

Figure 3. Intracellular formation of molecular assemblies. A) 24 h cytotoxicity of different molecules against HeLa cells. B) Flow cytometry analysis of HeLa cells treated with D-LTP (500×10^{-6} M) and D-LTPS (500×10^{-6} M) for 2 h. C) Confocal laser scanning microscopy images of HeLa cells treated with fL-LTP (100×10^{-6} M) and fD-LTP (100×10^{-6} M) for 2 and 24 h. D) Effect of endocytosis inhibitors (amiloride 25×10^{-6} M; chlorpromazine 15×10^{-6} M; EIPA 25×10^{-6} M; filipin III 3×10^{-6} M) on cellular uptake of fD-LTP that analyzed by flow cytometry. E–G) Representative Bio-TEM images of HeLa cells treated with: E) culture medium, F) D-LTP (500×10^{-6} M), and G) D-LTPS (500×10^{-6} M) for 24 h. Scale bars in (E–G): 2 μm in the low-magnification images, and 200 nm in the high-magnification images. Data are means ± standard deviation (SD), $^{**}P < 0.01$ (analysis of variance (ANOVA) and two-tailed Student's *t*-test).

especially for the cells treated with D-LTPS. Nec-1 could also rescue the cell viability from 50% to 100% that treated with D-LTPS at higher concentration (500×10^{-6} M) for 24 h, suggesting the leading cause of cell death induced by D-LTPS is necroptosis. We also employed HS-5 (Human bone marrow stromal cells) cell line as a normal cell model. The results (Figure S13, Supporting Information) indicate that the molecules are innocuous to normal cells even at high concentration (500×10^{-6} M), suggesting the cancer cell selectivity of our strategy.

To directly image the intracellular formation of molecular assemblies and their cellular distribution in living cells, we synthesized fluorophore-labeled peptide f-LTP (Figure S14, Supporting Information) by attaching nitrobenzofurazan (NBD) at ε-amine of lysine because NBD is an environment-sensitive fluorophore and has been employed for imaging biological components and molecular assemblies in the living system.[19] f-LTP exhibits similar self-assembling behaviors with LTP, forming nanoparticles at pH 7.4 and transforming to nanofibers at pH 5.0 (Figure S14, Supporting Information). The pH-dependent property ensures the morphology transformation of molecular assemblies of f-LTP in the lysosome of living cells. Time-dependent confocal laser scanning microscopy (CLSM) showed that the green fluorescence from intracellular assemblies formed by f-LTP colocalized with the red fluorescence from the lysosome in HeLa cells at first 2 h (Figure 3C), indicating the lysosomal formation of molecular assemblies that initiated by lysosomal acidic environment. The results also suggest that lysosomes of HeLa cells treating with fD-LTP swell and become enlarged dramatically. The enlargement of lysosomal volume also increases the intensity of cytosolic fluorescence of assemblies, indicating the molecular assemblies could escape from the lysosome. Compared with fL-LTP-treated cells, the intensity of fluorescence from the cells treated with fD-LTP is much higher, which could be due to the intracellular stability of fD-LTP. With the increase of incubation time (24 h), the lysosome volume of cells treated with fD-LTP becomes much larger, suggesting the sustainable accumulation of molecular assemblies. According to the cytotoxicity of molecules to normal cell HS-5, we further investigate the cellular uptake of self-assembly molecules (Figure S15, Supporting Information) by normal cells. CLSM images indicate that tumor cells uptake more nanoparticles than the normal cells does, which may explain why the self-assembly molecules exhibit innocuous to normal cells.

To understand the modes of endocytosis involved in the uptake of molecules by HeLa cells, we employed inhibitors of different endocytic processes to determine the cellular uptake pathways (Figure 3D). The results show that the addition of amiloride (an inhibitor of macropinocytosis) and chlorpromazine (an inhibitor of clathrin-mediated endocytosis) hardly affects the uptake of fD-LTP. Co-incubation of 5-(*N*-ethyl-*N*-isopropyl)-amiloride (EIPA), another inhibitor of macropinocytosis, reduces the uptake of fD-LTP for about 24% (analyzed by flow cytometry). Filipin III, an inhibitor of caveolae-mediated endocytosis by disrupting lipid raft, significantly decreases the uptake of fD-LTP by about 70%. These results indicated that the nanoparticles formed by LTP mainly undergo caveolae-mediated endocytosis, which ensures the further accumulation of LTP in lysosomes/endosomes after cellular uptake and then self-assemble to form the nanofibrous network under acidic conditions. To determine the concentration of peptide in lysosomes, we extracted the lysosomes of HeLa cells that were treated with peptides using a Lysosome Isolation Kit, and determined the concentration of peptides by LC-MS and TEM (Figure S16, Supporting Information). TEM imaging of extracted lysosomes shows the formation of nanofibrous network inside the lysosomes, further suggesting the formation of assemblies inside the lysosomes. LC-MS calculation indicates that the concentration of peptides inside the lysosomes is much higher than the CMC value in vitro, confirming that the accumulation of peptides inside the lysosome is sufficient to form assemblies in the lysosome. To prove the formation of the hydrogel like structure in living cells, we performed fluorescence recovery after photobleaching (FRAP) experiments (Figure S17, Supporting Information) by bleaching the Lysotracker Deep Red (DND-99) signal. Molecules in liquid phase undergo exchange rapidly with the surrounding cytoplasm, while molecules in hydrogel-like phase undergo a slower exchange. According to the FRAP results, the control group has a strong recovery of the fluorescence signal, with 68.3% ± 22.0%. While D-LTP- and D-LTPS-treated groups exhibited a poor FRAP recovery, with 40.0% ± 16.5% for D-LTP and 20.8% ± 7.9% for D-LTPS, respectively. These results suggested that D-LTP and D-LTPS form hydrogel-like structures in the lysosomes. We further investigated the nanostructures formed by LTP inside HeLa cells using Bio-TEM (Figure 3E–G). Compared with the control cells, the cells treated with D-LTP and D-LTPS show swollen and different shaped lysosomes (blue square frame in Figure 3), indicating lysosomal hydrogel could influence the integrity of the lysosome. Time-dependent bio-TEM (Figure 3E–G; and Figure S19, Supporting Information) reveals the gradual formation of nanofibers inside the lysosome. After 24 h incubation, TEM results show obvious nanofiber formation in the lysosome (as indicated by red arrow), suggesting the morphology transformation of LTP under the acidic condition in the lysosome. We also found the cytoplasmic nanofibers with the extension of incubation time, indicating the molecular assemblies could escape from the lysosome into the cytoplasm with the increase of incubation time.

2.3. Lysosomal Hydrogelation Improves Chemosensitivity of Conventional Chemotherapy Drug in MDR Cells

MDR is one of the main obstacles for clinical chemotherapy failure and exists in almost all types of cancer cells and occurrence in all modes of treatment.[46,47] Lysosomal sequestration of lipophilic, weakly basic anticancer drugs is one of the mechanisms of MDR, which causes drug resistance by reducing drug availability to the active site.[48,49] To enhance the therapeutic effect of chemotherapeutic agents by eliminating lysosomal sequestration, several strategies, including lysosome alkalinizing agents and lysosomotropic agents, have been explored to reverse lysosomal drug accumulation. Induction of LMP by these small molecules is the direct consequence for enhancing the efficiency of chemotherapy drugs. Different from these strategies and based on the above results, we hypothesized that the lysosomal hydrogelation could also improve the lysosome sequestration of clinical drugs by phase transition of peptides

in lysosome to modulate the properties of the lysosome and inducing LMP (**Figure 4**a).

We first utilized HeLa cervical cancer cells as a research cancer cell model and chose the lysosomal sequestration drug doxorubicin (Dox) as the model drug (Figure 4B).[50] In the Dox-treated HeLa cells, CLSM results show that the fluorescent intensity of Dox is significantly reduced with the incubation time from 2 to 24 h. We hardly observe any fluorescence of Dox in the

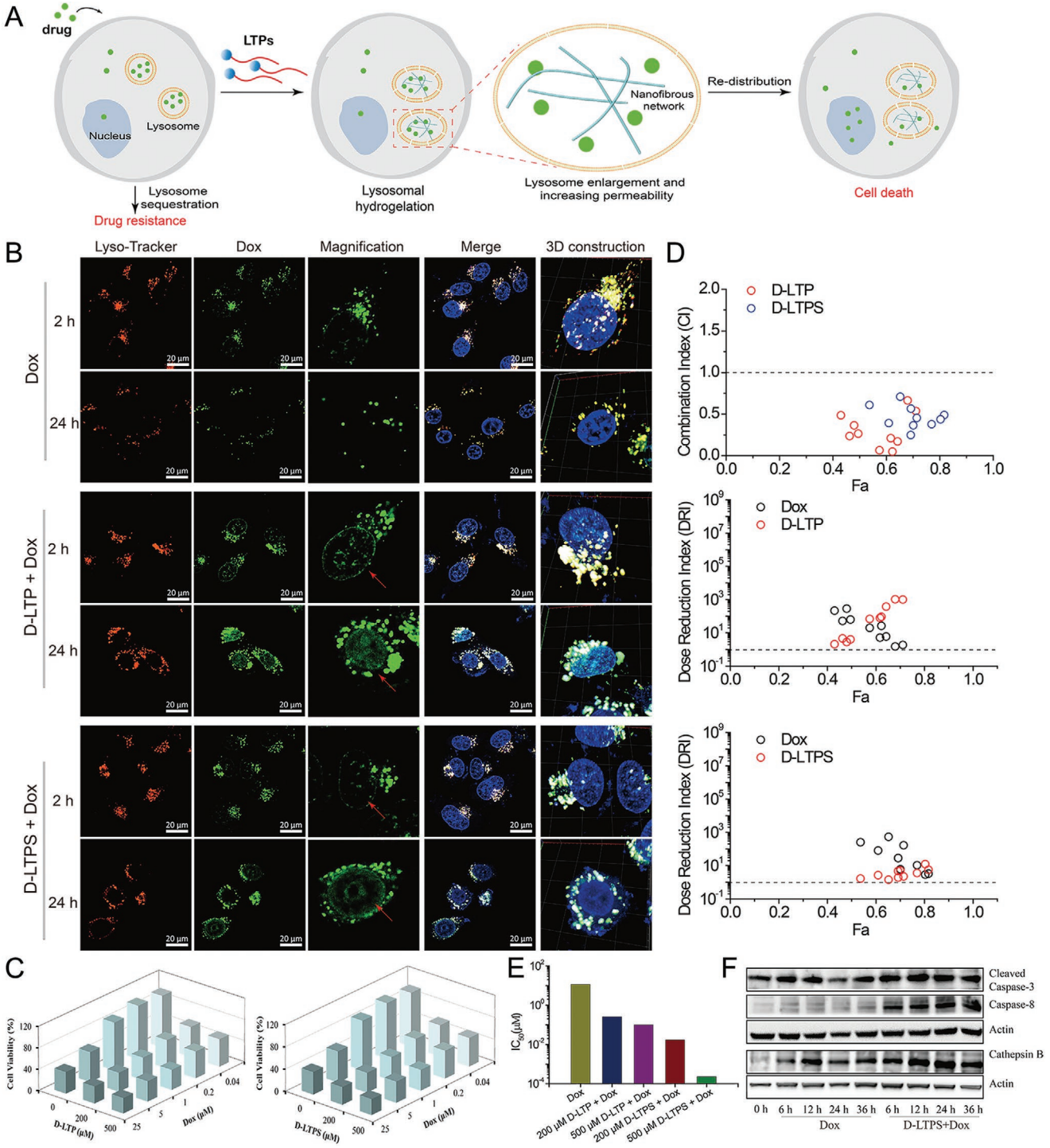

Figure 4. Synergistic effect of peptides and chemotherapeutic drug Doxorubicin. A) Schematic illustration of the synergistic effect of anticancer drug and peptides. B) CLSM images of HeLa cells treated with 5×10^{-6} M Dox and 500×10^{-6} M D-LTP or D-LTPS for 2 and 24 h. Lysosomes are stained with Lyso–Tracker, which denoted with red signals; Dox is presented as green signals. C) Combined cytotoxicity of peptides D-LTP or D-LTPS (200 and 500×10^{-6} M) with Dox after 24 h incubation. D) Combination index (CI) and dose-reduction index (DRI) calculated by the Chou–Talalay method.[52] E) IC_{50} of Dox of different groups. F) Expression level of cleaved Caspase-3, Caspase-8, and Cathepsin B in HeLa cells treated with Dox, and D-LTPS + Dox after 6, 12, 24, and 36 h incubation.

nucleus of HeLa cells and only observe fluorescent dots that colocalize with lyso-tracker. In contrast, the HeLa cells treated with Dox in the presence of D-LTP and D-LTPS exhibit much stronger green fluorescence from Dox. As shown in Figure 4B, CLSM images indicate that the green fluorescence occurs inside the nucleus at first 2 h, the intensity of which became much stronger with the increase of incubation time (24 h, red arrows). These results suggest that intracellular hydrogelation could increase Dox accumulation and endow drug escaping from lysosome sequestration to the active sites (e.g., nucleus).

We next evaluated the therapeutic effect of molecular assemblies and chemotherapy drug Dox (Figure 4C; and Figure S20, Supporting Information). The cytotoxicity results show that D-LTP and D-LTPS could significantly enhance the inhibitory effect of Dox against HeLa cells, indicating the synergistic effect of the combination of intracellular hydrogelation and Dox. In addition, the synergistic effect of molecular assemblies and Dox is also reflected in the reduction of IC_{50} of Dox (Figure 4E). The IC_{50} value of Dox is 11.35×10^{-6} M against HeLa cells. In contrast, adding D-LTP or D-LTPS (200×10^{-6} M) reduces the IC_{50} of Dox to 0.25×10^{-6} M or 16.8×10^{-9} M, which is about 45 and 676 folds reduction compared with the IC_{50} of Dox, respectively. These results indicate that the drug concentration needed to achieve the same therapeutic effect is significantly lower with intracellular hydrogelation than that in the Dox-treated group. Then we calculated the combination index (CI) and dose-reduction index (DRI) to evaluate the synergistic effect of assemblies and Dox (Figure 4D). CI depicts synergism ($CI < 1$), additive effect ($CI = 1$), and antagonism ($CI > 1$). The results indicate that all of the combination groups are less than 1, and most are less than 0.5, indicating a strong synergistic effect between molecular assemblies and Dox. DRI indicates dose-reduction folds for each drug in their combination form compared to the drug alone. Favorable DRI (> 1) indicates dose-reduction in the combination therapy, and almost all of the combination group's DRI is greater than 1, suggesting the lysosomal assemblies can promote the therapeutic efficiency of Dox. For D-LTPS, it can achieve a good therapeutic efficiency with Dox even at a low concentration of 20×10^{-6} M, which reduced the IC_{50} value of Dox for about 18 folds, indicating a strong synergistic effect between D-LTPS and Dox (Figure S21, Supporting Information). To further evaluate whether D-LTP and D-LTPS could improve the anticancer efficiency of Dox on drug-resistance cell lines, we further chose HepG2 and MCF-7 cell lines, and the corresponding anti-drug resistance (ADR) cell lines as research model (Figures S22–S25, Supporting Information). According to the results of combined cytotoxicity of HepG2 cells, the addition of D-LTP and D-LTPS achieves ten and eight folds reduction of IC_{50} of Dox, respectively. While for HepG2/ADR cells, D-LTP and D-LTPS achieves 15 and 588 folds reduction of IC_{50} of Dox. Moreover, for MCF-7, the addition of D-LTP and D-LTPS achieves two and seven folds reduction of IC_{50} of Dox, while for MCF-7/ADR cells, D-LTP and D-LTPS achieves 10 and 31 folds reduction of IC_{50} of Dox. These results indicate that our strategy could improve the anticancer efficiency of Dox, especially in the treatment of ADR cells.

We further investigate the mechanism of apoptosis by detecting the expression level of Cathepsin B, Caspase-3, and Caspase-8 by Western blotting experiments. According to previous research, tumor necrosis factor (TNF) induces an increased expression level of Cathepsin B, and Cathepsin B acts as an essential downstream mediator of TNF-triggered apoptosis.[51] Caspase-3 and Caspase-8 are normal proteases activated in the apoptosis pathway. Figure 4F shows that the expression level of cathepsin B peaked at 12 h, and the cells treated with the mixture of assemblies and Dox express a higher level of cathepsin B than the cells treated with Dox. Western blotting results also indicate that the HeLa cells treated with the mixture of assemblies and Dox express high levels of cleaved caspase-3 and caspase-8, suggesting cell death induced by the combination of molecular assemblies and Dox involved apoptosis.

2.4. Intracellular Assemblies Inhibit Tumor Growth and Boost Activity of Dox in Tumor-Bearing Mice

Based on the above encouraging results, we evaluated the therapeutic efficacy of LTP in the tumor-bearing mouse model. We first evaluated the biodistribution of assemblies by cyanine5.5 (Cy5.5) labeled peptides D-LTP-Cy5.5 and D-LTPS-Cy5.5 (**Figure 5**A). The biodistribution is carried out in the HeLa-cells-bearing tumor mouse model, which is developed by subcutaneous injection of 2×10^6 HeLa cells to the flank of the forelegs of nude mice. After the tumor reached to the average size of 200 mm^3, we injected free Cy5.5, D-LTP-Cy5.5, and D-LTPS-Cy5.5 intravenously through the tail vein and examined the fluorescence signals at the designated time. The in vivo imaging results show that the fluorescence signals in organs of Cy5.5-treated mice reduce significantly after injection, while the fluorescence intensity of D-LTP-Cy5.5- and D-LTPS-Cy5.5-treated mice are much higher than that of the free Cy5.5. The decrease of fluorescent intensity is relatively insignificant with the increase of administration time. The long retention time of the fluorescence from D-LTP-Cy5.5 and D-LTPS-Cy5.5 at the tumor sites confirms the ability of assemblies to prolong the retention time at tumor sites, thereby enhancing the therapeutic effect. We next utilized the ex vivo imaging to measure the fluorescence intensity of each group at tumor sites. After 4 h postinjection, mice were sacrificed, and the major organs and blood were collected for fluorescence imaging ($n = 3$) (Figure 5B). The ex vivo imaging results indicate that the fluorescence signals of D-LTP-Cy5.5 and D-LTPS-Cy5.5 at tumor sites are higher than that from the free-Cy5.5-treated group, which are 2.6- and 3.2-fold higher than the free-Cy5.5-treated one, respectively, indicating the accumulation of assemblies at tumor sites. In contrast, the free-Cy5.5-administered group is excreted rapidly by the kidney.

We next investigate the therapeutic effect of intracellular assemblies and their ability for addressing MDR in HeLa cells bearing tumor model (Figure 5C–E). Mice were randomly divided into 6 groups ($n = 5$), and treated with saline, Dox, D-LTP, D-LTPS, D-LTP + Dox, and D-LTPS + Dox, respectively. Figure 5A shows that the combination group of D-LTPS and Dox exhibits a significant inhibiting effect on the tumor growth after the first administration, the antitumor effect sustained for the whole therapeutic period. In contrast, the treatments of the combination of D-LTP and Dox show feeblish inhibition on the tumor growth. Specifically, the combination of D-LTP and Dox showed some inhibiting effect at the first 6 days, but the tumors had a significant growth rate in the following treatment. Administration of D-LTPS alone has similar antitumor effects with Dox at first 10 days, while D-LTP has some effects on preventing tumor growth. At the end of the

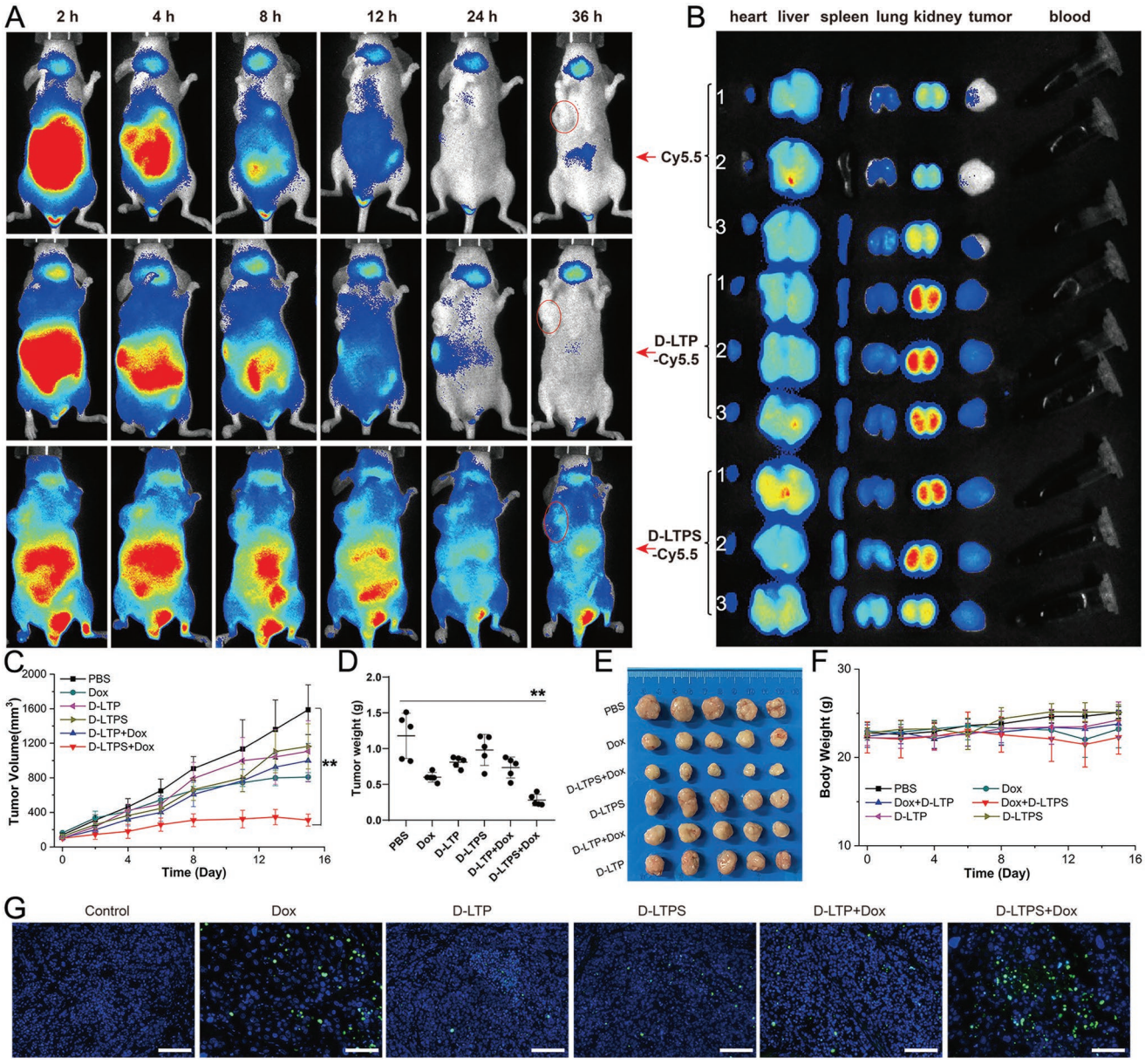

Figure 5. The in vivo therapeutic efficacy of peptides and anticancer drug Doxorubicin on tumor growth in a subcutaneous HeLa tumor model. A) In vivo distribution of Cy5.5, D-LTP-Cy5.5, and D-LTPS-Cy5.5 in the HeLa tumor model at different timepoints. B) The ex vivo distribution of Cy5.5, D-LTP-Cy5.5, and D-LTPS-Cy5.5 in the HeLa cell tumor model. C) The tumor growth profiles of each group (n = 5). D) The relative tumor weights of each group (n = 5). E) Images of tumor issue of each group (n = 5). F) The body weight profiles of each group (n = 5). G) TUNEL results of tumor tissue for each group; scale bar: 200 µm.

treatment, we collected major organs of each group and weight the tumor plagues to calculate the therapeutic effect. We further used histopathological analysis by H&E staining and TUNEL assays (Figure 5G; and Figure S26, Supporting Information) to evaluate the toxicity of assemblies on major organs and their antitumor effect. Compared with the saline-treated group, the treatment of D-LTPS + Dox shows a 76.2% inhibition of tumor growth, which exhibits significant anti-tumor ability. In addition, there are no significant changes in body weights during the treatment period. H&E staining indicates no obvious damage to the heart, liver, spleen, lung, and kidney. TUNEL assays show that the combination of D-LTPS and Dox exhibits obvious apoptosis of tumor tissue compared to other groups, confirming the antitumor efficacy of the combination therapy of intracellular assemblies and chemotherapy drugs. These results suggest that intracellular assemblies could effectively sensitize tumors to Dox administration and boost its activity toward MDR cancers. We also evaluated in vivo tolerance of the peptides via i.v. injection. The results show that injection of peptide (D-LTP or D-LTPS) at a single dose of 200 mg kg^{-1} is fatal to mice. An i.v. injection of peptides at a single dose of 150 mg kg^{-1} is healthy to mice, as evidenced by histological examination of major organs (Figure S27, Supporting Information), indicating the fatal dosage of our peptide is higher than 150 mg kg^{-1}, which is at least 5 times higher than the dosage for cancer therapy.

2.5. Lysosomal Assemblies Boost the Activity of Sunitinib Against Sunitinib-Resistant Ovarian Cancer

To further investigate whether the strategy could improve the MDR in severe tumors (e.g., ovarian cancer), we examine their effect in sunitinib resistance ovarian cancer SK-OV-3 since sunitinib induces lysosome-dependent MDR.[49] CLSM results show that intracellular assemblies formed by LTP-NBD (green fluorescence) colocalized with the lysosomes (red fluorescence) in SK-OV-3 cells at first 2 h incubation (**Figure 6**A). With the increase of incubation time (24 h), the lysosomes become much larger, similar to the observation in HeLa cells. We also observe

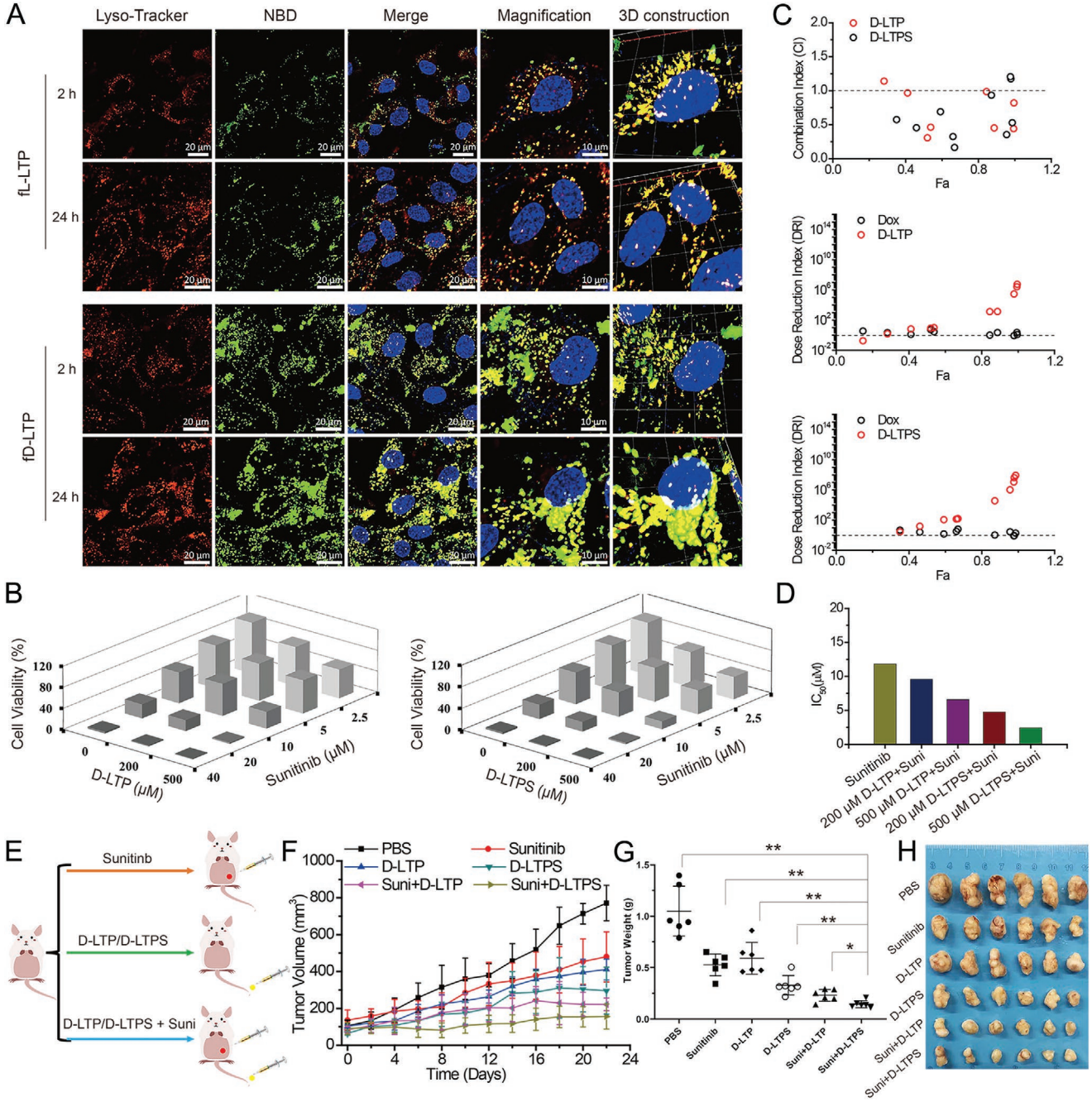

Figure 6. Cellular uptake and combination therapy of sunitinib and assemblies in SK-OV-3 ovarian cancer model. A) CLSM images of SK-OV-3 cells treated with fL-LTP (100×10^{-6} M) and fD-LTP (100×10^{-6} M) for 2 and 24 h. B) Combination therapy of peptides D-LTP (or D-LTPS) and sunitinib against SK-OV-3 cells after 48 h incubation. C) Combination index (CI) and dose-reduction index (DRI) calculated according to the Chou–Talalay method.[52] D) Summary of the IC_{50} of different groups against SK-OV-3 cells. E) Schematic illustration of the treatments. Sunitinib is administered intraperitoneally and peptides are administered intravenously every other day. F) Tumor growth profiles from each group in SK-OV-3 cell tumor model ($n = 6$). G) Tumor weight measurements in SK-OV-3-induced tumor model ($n = 6$). H) Typical image of tumor mass from each group in SK-OV-3-induced tumor model ($n = 6$).

some cytoplasmic fluorescence after 24 h incubation, suggesting the assemblies could also escape from the lysosome of SK-OV-3 cells. We then examine the therapeutic effect of D-LTP, D-LTPS, and their combination effect with sunitinib in SK-OV-3 cancer cells. The results indicate that the combination of assemblies with sunitinib inhibits SK-OV-3 cell growth more efficiently than sunitinib itself (Figure 6B). The combination of D-LTP (or D-LTPS) and sunitinib (10×10^{-6} M) inhibits 67.7% (85.3%) of SK-OV-3 cells. In contrast, sunitinib inhibits only 41.0% SK-OV-3 cells, and the peptides are almost innocuous to the cells. We evaluated the synergistic effect of assemblies and sunitinib by calculating the CI and DRI. The results show that most CI data are less than 1, while all DRI data are greater than 1, indicating a strong synergistic effect between molecular assemblies and sunitinib (Figure 6C). According to the DRI diagram, D-LTP and D-LTPS could cause three folds and 1000 folds dose-reduction for 90% inhibitory effect toward SK-OV-3 cells than sunitinib does, respectively. The IC_{50} (Figure 6D) values of sunitinib, D-LTP + sunitinib, and D-LTPS + sunitinib against SK-OV-3 cells are 1180, 657, and 244×10^{-9} M, respectively, indicating the synergistic effect of molecular assemblies and sunitinib.

Then we investigated the in vivo therapeutic effect of intracellular assemblies and sunitinib in SK-OV-3-bearing tumor mouse model. We randomly divided tumor-bearing mice into 6 groups ($n = 6$), and treated them with PBS, sunitinib, D-LTP, D-LTPS, D-LTP + sunitinib, and D-LTPS + sunitinib every other day, respectively. As shown in Figure 6F, the tumor sizes reduced obviously in the D-LTP + sunitinib- and D-LTPS + sunitinib-treated groups, while the inhibition effect is moderate in sunitinib-, D-LTP-, and D-LTPS-treated groups. Compared with the PBS group, sunitinib, D-LTP, and D-LTPS inhibit tumor growth by 37.88%, 46.77%, and 61.70%, respectively. The inhibitory effect on the tumor growth of D-LTP + sunitinib and D-LTPS + sunitinib groups exists persistently during the treatment period, promoting an overall inhibition of 71.32% and 79.80% in tumor growth. After the treatment, all mice were sacrificed, and all tumor mass and organs were collected. We weighted the tumor mass of each group and verified the therapeutic efficacy of D-LTP + Sunitinib and D-LTPS + Sunitinib, which showed 76.87% and 85.53% inhibition of tumor growth, respectively. The therapeutic effect of the groups treated with sunitinib, D-LTP, and D-LTPS is 49.84%, 43.75%, and 68.63% (Figure 6G,H), respectively. The body weight of each group showed no significant reduction during the treatment process and the H&E staining of each tissue did not show any obvious damage (Figure 6I; and Figure S28, Supporting Information), indicating the biocompatibility of the treatment toward major organs. These results suggest that the intracellular assemblies play an essential role in improving the therapeutic efficiency of the current chemotherapeutic drugs against MDR.

3. Conclusion

This work reports an artificial biomolecular condensate formed through proton-induced phase transformation of peptide spatiotemporally in the lysosome of cancer cells. Lysosomal assemblies cause the enlargement of the lysosome, which changes the permeability of lysosome and further redirects the distribution of current chemotherapy drugs. We demonstrated that the redistribution of anticancer drugs could significantly increase their efficiency in MDR cancer cells and tumor-bearing mouse models. Compared with the reported strategies for addressing MDR, this work is the first example of using lysosomal hydrogelation to redirect the chemotherapeutics that sequestrated inside lysosome to the organelle where the target is, which opens up a new adventure for improving the drug efficiency related to lysosome sequestration. We envision that the strategy demonstrated here could also be suitable for other stimuli (enzyme, redox, light, and ionic strength) to induce biomolecular condensates formation in different organelles and for different functions.[53]

Supporting Information

Supporting Information is available from the Wiley Online Library or from the author.

Acknowledgements

This project was supported by Westlake Education Foundation and Tencent Foundation, the National Natural Science Foundation of China (No. 82022038). The authors thank Instrumentation and Service Center for Physical Sciences and the CryoEM facility at Westlake University for the assistance work in measurement. Mice were handled in accordance with institutional guidelines, and all animal studies were approved by the Institutional Animal Care and Use Committee (IACUC) of Westlake University (IACUC Protocol #20-016-WHM).

Conflict of Interest

The authors declare no conflict of interest.

Data Availability Statement

Research data are not shared.

Keywords

hydrogels, lysosomal membrane permeabilization, multidrug resistance, peptides, self-assembly

Received: June 19, 2021
Revised: August 19, 2021
Published online: October 10, 2021

[1] G. M. Whitesides, B. Grzybowski, *Science* **2002**, *295*, 2418.
[2] T. Aida, E. W. Meijer, S. I. Stupp, *Science* **2012**, *335*, 813.
[3] M. E. Davis, P. C. H. Hsieh, T. Takahashi, Q. Song, S. Zhang, R. D. Kamm, A. J. Grodzinsky, P. Anversa, R. T. Lee, *Proc. Natl. Acad. Sci. USA* **2006**, *103*, 8155.
[4] A. F. Dexter, A. S. Malcolm, A. P. J. Middelberg, *Nat. Mater.* **2006**, *5*, 502.
[5] S. Zhang, *Nat. Biotechnol.* **2003**, *21*, 1171.
[6] R. V. Ulijn, A. M. Smith, *Chem. Soc. Rev.* **2008**, *37*, 664.
[7] T. Aida, E. Meijer, S. Stupp, *Science* **2012**, *335*, 813.

[8] C. Yuan, W. Ji, R. Xing, J. Li, E. Gazit, X. Yan, *Nat. Rev. Chem.* **2019**, *3*, 567.
[9] J. Boekhoven, W. E. Hendriksen, G. J. Koper, R. Eelkema, J. H. van Esch, *Science* **2015**, *349*, 1075.
[10] D. J. Smith, G. A. Brat, S. H. Medina, D. Tong, Y. Huang, J. Grahammer, G. J. Furtmüller, B. C. Oh, K. J. Nagy-Smith, P. Walczak, *Nat. Nanotechnol.* **2016**, *11*, 95.
[11] H. Shigemitsu, I. Hamachi, *Acc. Chem. Res.* **2017**, *50*, 740.
[12] Z. Feng, T. Zhang, H. Wang, B. Xu, *Chem. Soc. Rev.* **2017**, *46*, 6470.
[13] G. Liang, H. Ren, J. Rao, *Nat. Chem.* **2010**, *2*, 54.
[14] R. A. Pires, Y. M. Abul-Haija, D. S. Costa, R. Novoa-Carballal, R. L. Reis, R. V. Ulijn, I. Pashkuleva, *J. Am. Chem. Soc.* **2015**, *137*, 576.
[15] J. Gao, J. Zhan, Z. Yang, *Adv. Mater.* **2020**, *32*, 1805798.
[16] P.-P. He, X.-D. Li, L. Wang, H. Wang, *Acc. Chem. Res.* **2019**, *52*, 367.
[17] A. Tanaka, Y. Fukuoka, Y. Morimoto, T. Honjo, D. Koda, M. Goto, T. Maruyama, *J. Am. Chem. Soc.* **2015**, *137*, 770.
[18] H.-W. An, L.-L. Li, Y. Wang, Z. Wang, D. Hou, Y.-X. Lin, S.-L. Qiao, M.-D. Wang, C. Yang, Y. Cong, Y. Ma, X.-X. Zhao, Q. Cai, W.-T. Chen, C.-Q. Lu, W. Xu, H. Wang, Y. Zhao, *Nat. Commun.* **2019**, *10*, 4861.
[19] Y. Gao, J. Shi, D. Yuan, B. Xu, *Nat. Commun.* **2012**, *3*, 1033.
[20] D.-B. Cheng, D. Wang, Y.-J. Gao, L. Wang, Z.-Y. Qiao, H. Wang, *J. Am. Chem. Soc.* **2019**, *141*, 4406.
[21] H. Wu, M. Fuxreiter, *Cell* **2016**, *165*, 1055.
[22] H. Strickfaden, T. O. Tolsma, A. Sharma, D. A. Underhill, J. C. Hansen, M. J. Hendzel, *Cell* **2020**, *183*, 1772.
[23] A. Molliex, J. Temirov, J. Lee, M. Coughlin, A. P. Kanagaraj, H. J. Kim, T. Mittag, J. P. Taylor, *Cell* **2015**, *163*, 123.
[24] P. Li, S. Banjade, H.-C. Cheng, S. Kim, B. Chen, L. Guo, M. Llaguno, J. V. Hollingsworth, D. S. King, S. F. Banani, P. S. Russo, Q.-X. Jiang, B. T. Nixon, M. K. Rosen, *Nature* **2012**, *483*, 336.
[25] M. Kato, S. L. McKnight, *Annu. Rev. Biochem.* **2018**, *87*, 351.
[26] H. Nakamura, A. A. Lee, A. S. Afshar, S. Watanabe, E. Rho, S. Razavi, A. Suarez, Y.-C. Lin, M. Tanigawa, B. Huang, R. DeRose, D. Bobb, W. Hong, S. B. Gabelli, J. Goutsias, T. Inoue, *Nat. Mater.* **2018**, *17*, 79.
[27] I. Kwon, S. Xiang, M. Kato, L. Wu, P. Theodoropoulos, T. Wang, J. Kim, J. Yun, Y. Xie, S. L. McKnight, *Science* **2014**, *345*, 1139.
[28] L. Tang, *Nat. Methods* **2019**, *16*, 23.
[29] C. de Duve, *Nat. Cell Biol.* **2005**, *7*, 847.
[30] J. W. Coffey, C. De Duve, *J. Biol. Chem.* **1968**, *243*, 3255.
[31] S. R. Bonam, F. Wang, S. Muller, *Nat. Rev. Drug Discovery* **2019**, *18*, 923.
[32] L. N. Aldrich, S.-Y. Kuo, A. B. Castoreno, G. Goel, P. Kuballa, M. G. Rees, B. A. Seashore-Ludlow, J. H. Cheah, I. J. Latorre, S. L. Schreiber, A. F. Shamji, R. J. Xavier, *J. Am. Chem. Soc.* **2015**, *137*, 5563.
[33] B. Rathore, K. Sunwoo, P. Jangili, J. Kim, J. H. Kim, M. Huang, J. Xiong, A. Sharma, Z. Yang, J. Qu, J. S. Kim, *Biomaterials* **2019**, *211*, 25.
[34] M. Akishiba, T. Takeuchi, Y. Kawaguchi, K. Sakamoto, H. H. Yu, I. Nakase, T. Takatani-Nakase, F. Madani, A. Graslund, S. Futaki, *Nat. Chem.* **2017**, *9*, 751.
[35] N. Gong, Y. Zhang, X. Teng, Y. Wang, S. Huo, G. Qing, Q. Ni, X. Li, J. Wang, X. Ye, T. Zhang, S. Chen, Y. Wang, J. Yu, P. C. Wang, Y. Gan, J. Zhang, M. J. Mitchell, J. Li, X.-J. Liang, *Nat. Nanotechnol.* **2020**, *15*, 1053.
[36] H. Wang, Z. Feng, B. Xu, *Angew. Chem., Int. Ed.* **2019**, *58*, 10423.
[37] A. M. Kaufmann, J. P. Krise, *J. Pharm. Sci.* **2007**, *96*, 729.
[38] R. Halaby, *Cancer Drug Resist.* **2019**, *2*, 31.
[39] M. R. Sawaya, S. Sambashivan, R. Nelson, M. I. Ivanova, S. A. Sievers, M. I. Apostol, M. J. Thompson, M. Balbirnie, J. J. W. Wiltzius, H. T. McFarlane, A. Ø. Madsen, C. Riekel, D. Eisenberg, *Nature* **2007**, *447*, 453.
[40] S. J. Roeters, M. Sawall, C. E. Eskildsen, M. R. Panman, G. Tordai, M. Koeman, K. Neymeyr, J. Jansen, A. K. Smilde, S. Woutersen, *Biophys. J.* **2020**, *119*, 87.
[41] M. Ma, Y. Kuang, Y. Gao, Y. Zhang, P. Gao, B. Xu, *J. Am. Chem. Soc.* **2010**, *132*, 2719.
[42] D. J. Adams, M. F. Butler, W. J. Frith, M. Kirkland, L. Mullen, P. Sanderson, *Soft Matter* **2009**, *5*, 1856.
[43] A. Degterev, Z. Huang, M. Boyce, Y. Li, P. Jagtap, N. Mizushima, G. D. Cuny, T. J. Mitchison, M. A. Moskowitz, J. Yuan, *Nat. Chem. Biol.* **2005**, *1*, 112.
[44] C. Huang, Y. Luo, J. Zhao, F. Yang, H. Zhao, W. Fan, P. Ge, *PLoS One* **2013**, *8*, e66326.
[45] C. W. Davies, J. Chaney, G. Korbel, D. Ringe, G. A. Petsko, H. Ploegh, C. Das, *Bioorg. Med. Chem. Lett.* **2012**, *22*, 3900.
[46] B. C. Baguley, *Mol. Biotechnol.* **2010**, *46*, 308.
[47] G. Szakács, J. K. Paterson, J. A. Ludwig, C. Booth-Genthe, M. M. Gottesman, *Nat. Rev. Drug Discovery* **2006**, *5*, 219.
[48] K. J. Gotink, H. J. Broxterman, M. Labots, R. R. de Haas, H. Dekker, R. J. Honeywell, M. A. Rudek, L. V. Beerepoot, R. J. Musters, G. Jansen, A. W. Griffioen, Y. G. Assaraf, R. Pili, G. J. Peters, H. M. W. Verheul, *Clin. Cancer Res.* **2011**, *17*, 7337.
[49] B. Zhitomirsky, Y. G. Assaraf, *Oncotarget* **2015**, *6*, 1143.
[50] T. Yamagishi, S. Sahni, D. M. Sharp, A. Arvind, P. J. Jansson, D. R. Richardson, *J. Biol. Chem.* **2013**, *288*, 31761.
[51] L. Foghsgaard, D. Wissing, D. Mauch, U. Lademann, L. Bastholm, M. Boes, F. Elling, M. Leist, M. Jäättelä, *J. Cell Biol.* **2001**, *153*, 999.
[52] T.-C. Chou, *Cancer Res.* **2010**, *70*, 440.
[53] Y. Shin, J. Berry, N. Pannucci, M. P. Haataja, J. E. Toettcher, C. P. Brangwynne, *Cell* **2017**, *168*, 159.